Open-circuit fault detection of inverter fed PMSM for electrical powertrain applications

Fatima Haidar, Takwa Sellami Douiri, Thomas Bartoli
Hybrid Innovative Powertrain-Capgemini Engineering, Research and Innovation Direction, Meudon, France

Article Info

ABSTRACT

This paper aims to enhance the reliability of power electronic converters fed permanent magnet synchronous machine for electrical powertrain applications. Many faults like open circuit may affect the power converter and quickly lead to a decline in supplied power quality and all the power train components behavior. In this framework, this paper proposes an open circuit fault detection scheme for inverters. First, the dynamic models of the powertrain subsystems were developed. In fact, all the mathematics models of the motor, inverter, power converter, battery and charger are presented. Then, a detection scheme of open-circuit fault in inverter/motor. The control schemes were elaborated based on current analysis method. The diagnosis strategy under discontinuous switch-ing dynamics of the DC/AC inverter is proposed.

Corresponding Author:

Fatima Haidar
Hybrid Innovative Powertrain-Capgemini Engineering, Research and Innovation Direction
12 rue de la Verrerie, 92190, Meudon, France
Email: fatima.haidar@capgemini.com

1. INTRODUCTION

Energy and environmental issues currently represent major concerns at the international level. World population growth and the activity of the industrialized and emerging countries have led to an explosion in energy needs. The use of fossil resources is responsible for the majority of greenhouse gas emissions in the atmosphere, this pollution is at the root of the climatic upheavals we are facing today. In addition to the environmental impacts, fossil fuel reserves are limited and thus cannot meet global demand in the medium term. Of all the sectors implicated in these environmental problems, the automobiles are regularly mentioned; the number of vehicles on the road is constantly increasing. Thanks to government restrictions on pollution thresholds and technical innovations, manufacturers are moving towards technologies that emit fewer pollutants [1], [2]. The different cases for geopolitical or economic considerations are determining factors in the technological choices: types of electrical machines, arrangement of the battery pack or the battery cells, fuel cell technology and chemistry, and cooling systems. Hybrid electric vehicle (HEV) technologies offer a promising solution in this field and brings the "zero emission" propulsion target within reach. As a result, manufacturers must bring forward cutting-edge powertrain technologies to provide customers with compact, energy efficient, long-range, environmentally friendly cars at limited costs. This challenge requires a lot of research and development to design better technological solutions to fulfill the needs in low carbon emission transports necessary for slowing down global warming and improving cities air quality [3], [4].

This paper will focus on the electric motor for an electric vehicle powertrain. Alternative current (AC) motor drives components can suffer from failures as they wear out due to many factors such as overvoltage, high temperatures or mechanical vibrations. The failures can occur in the motor and in the static converter(s)

and more specifically in the subcomponents like sensors, power semi-conductors, and printed circuit boards [5]. This paper will also develop on a strategy to detect and solve these open circuit and short circuit faults and expose diagnosis methods. The mathematical models and controller designs used for the simulations are developed in the first part. The second part presents the strategy for solving open circuit faults and the last parts shows the software implementation aspects and the analyzed simulation results [6].

Power modules represent 34% of power converters failures and power converters contribute to 80% of total electric drives failures [1], [3]. Moreover, the power devices gathered with their gate drivers and control circuits represent 50% of the industrial power converters which shows the importance of those failures [7], [8]. Open-circuit (OC) and short-circuit are the two main types of failure occurring in power modules. OC faults do not damage harshly the power devices even though they produce distorted currents and thus create fast electromagnetic torque oscillations which cause mechanical stress. On the other hand, short circuit faults result in very high currents which leads to the overheating and failure of the power electronic devices within a very short time if they are not dealt with.

Diagnosis is done in three steps : detection, isolation and identification of the fault to respectively detect an unexpected behaviour, locate the faulty component and assess the type of fault and its severity [9], [10]. There are model-based diagnosis techniques which uses mathematical models of the plant with one or more observers and compare its(their) output(s) with measured states of the plant. This method requires a good enough observability of the system and an accurate model which might be tough or even impossible to derive for complex systems.

Active fault diagnosis is, contrary to the three others, an invasive technique that consists in adding a signal to the input of the system and extract its output to monitor the added input component impact. The controller proposed here is an indirect-field oriented (IFO) vector controller [11]. In the case of the permanent magnet synchronous machine (PMSM), the rotor flux fixed frame is the same as the rotor fixed frame since its magnets are responsible for the flux. The Park transform matrix is used for the controller design.

The three passive techniques can be combined into a hybrid diagnosis technique to remove some drawbacks that they present alone. Short circuit faults are very fast and destructive, so they are tackled by inverters built-in devices that shut down the converter when an overcurrent is detected. On the other hand, open-circuit (OC) faults might be longer to detect and don't automatically lead to a shutdown of the drives. This is mainly why faults detection and isolation (FDI) techniques focus on OC [7].

All the FDI techniques outlined above can be applied to electric drives. The goal is to design a detection and isolation algorithm that is robust against false alarms, and which does not depend on the operating conditions. Fault detection through monitoring of time signals can be done either with current or voltage signals even if voltage measurements require additional sensors, or less straightforward algorithms, and are then less common. The detection is either based on a complex pattern recognition algorithm or simply based on a specific value that dramatically changes when a fault occurs. Some methods rely on a Park transform of the measured currents and the measure of the derivative of the space vector phase. To compare reference and real currents is also a robust way to detect and isolate an OC fault [7].

Instead of just using measurements, a current observer can be used to compare its output with the measures. The resulting residual is compared to a threshold to perform detection and identification, like for the previous techniques. More complex techniques like artificial intelligence and neural networks were used also for FDI techniques related to electric drives [7], [12].

2. MATHEMATICAL MODELS
2.1. Electric motor
2.1.1. Physical model

The model of the permanent magnet synchronous motor (PMSM) is derived by applying Kirchhoff voltage law on the three phases and the energy conservation law for electromagnetic torque T_{em} derivation. Then by applying the Park transform to the three obtained electric equations and adding the mechanical equation, one gets the state-space equations for the PMSM in the rotor-fixed rotating frame [11]:

$$L_d \frac{di_d}{dt} = v_d - R_s i_d + L_q i_q w_r \qquad (1)$$

$$L_q \frac{di_q}{dt} = v_q - R_s i_q - L_d i_d w_r - \psi_m w_r \tag{2}$$

$$J \frac{dw_m}{dt} = T_{em} - T_f - T_L \tag{3}$$

where J is the total system inertia referred to the motor shaft, L_d and L_q are the motor inductances in the d and q directions respectively, R_s is the stator phase resistance, and T_{em}, T_f and T_L are the electromagnetic, friction and load torques respectively. i_d and i_q are the currents creating magnetic flux in the d and q directions respectively, w_r and w_m are the electrical and mechanical angular velocities respectively, linked by the number of pole pairs n_p :

$$w_r = n_p w_m \tag{4}$$

the electromagnetic torque and the friction torque formulas are :

$$T_{em} = \frac{3}{2} n_p (\psi_m i_q + (L_d - L_q) i_d i_q) \tag{5}$$

$$T_f = b_{lin} w_m + b_{qu} w_m^2 \tag{6}$$

where b_{lin} and b_{qu} are the linear and quadratic friction coefficients respectively, and Psi_m is the flux linkage between the PMs and the stator.

2.1.2. Controller design

When expressed in the Park frame, the abc sinusoidal quantities become constant (at steady-state), and then far easier to track for a linear proportional integrator (PI) controller. Besides, as mechanical dynamics are far slower than electrical dynamics, w_r can be considered as a slowly varying parameter and then, the electrical equations can be studied as linear ones for control purposes. By replacing the derivatives with the Laplace operator p in (1) and (2) and putting the result into a compact matrix form, one gets (7).

$$\underbrace{\begin{pmatrix} i_d \\ i_q \end{pmatrix}}_{\mathbf{i_{dq}}} = \underbrace{\begin{bmatrix} pL_d + R_s & -L_q w_r \\ L_d w_r & pL_q + R_s \end{bmatrix}^{-1}}_{\mathbf{G}} \underbrace{\left(\begin{bmatrix} v_d \\ v_q \end{bmatrix} - \begin{bmatrix} 0 \\ \psi w_r \end{bmatrix} \right)}_{\mathbf{v_{dq} - E}} \tag{7}$$

It is a system of two coupled first order ordinary differential equations. In order to use two PI controller for id^* and iq^* references, it is useful to decouple the equations thanks to an inner feedback loop, as proposed in [13], [14], with added "active damping" fictitious resistances for external disturbances and modeling errors rejection. The estimated parameters used by the controller will have the hat notation within this paper. The decoupling inner feedback and the PI controller are given by (8). The block diagram of the whole system is shown in Figure 1.

$$W = \begin{pmatrix} -R_{a,d} & -\hat{L}_q w_r \\ \hat{L}_d w_r & -R_{a,q} \end{pmatrix} \quad ; \quad F = \begin{pmatrix} k_{p,d} + k_{i,d}/p & 0 \\ 0 & k_{p,q} + k_{i,q}/p \end{pmatrix} \tag{8}$$
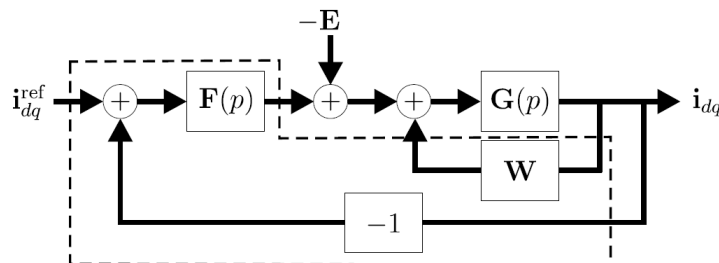

Figure 1. Closed loop current control block diagram [13]

The internal feedback loop and the regulator PI controller are designed so that the closed-loop system behaves like two decoupled one dimensional first-order systems with bandwidth α_c:

$$G_{cl} = G'F(I + G'F)^{-1} = \begin{bmatrix} \frac{\alpha_c}{p+\alpha_c} & 0 \\ 0 & \frac{\alpha_c}{p+\alpha_c} \end{bmatrix} \quad ; \quad G' = G(I + GW)^{-1} \tag{9}$$

if we consider no parameter estimation errors, firstly i_d and i_q dynamics are decoupled, and secondly the targeted dynamics can be achieved by pole placement by setting:

$$k_{p,d} = \alpha_c \hat{L}_d \quad k_{i,d} = \alpha_c (\hat{R}_s + R_{a,d}) \tag{10}$$

$$k_{p,q} = \alpha_c \hat{L}_q \quad k_{i,q} = \alpha_c (\hat{R}_s + R_{a,q}) \tag{11}$$

finally, the active resistance are chosen in such a way that the disturbance and modeling errors rejection dynamics are as fast as the closed loop dynamics [13]:

$$R_{a,d} = \alpha_c \hat{L}_d - \hat{R}_s \quad R_{a,q} = \alpha_c \hat{L}_q - \hat{R}_s \tag{12}$$

one can choose the bandwidth by using its link to the rise time of a first order system is given by (13).

$$\alpha_c = \frac{\ln(9)}{t_{r,c}} \tag{13}$$

The current controller outputs a voltage reference:

$$vdq^* = F(idq^* - idq) + Widq \tag{14}$$

as explained later for the inverter and its control, the voltage reference magnitude must be limited to a value V_{max}. When the reference magnitude exceeds V_{max}, the controller reacts:

$$v_{d,sat}^* = \frac{V_{max}v_d^*}{|v_{dq}^*|} \quad ; \quad v_{q,sat}^* = \frac{V_{max}v_q^*}{|v_{dq}^*|} \tag{15}$$

because of this control structure having an internal saturation, anti wind-up must be implemented for both the d and q PI controllers to counteract an irrelevant rise of the PI integrators that could occur when $|vdq^*|$ is above V_{max} and that leads to overshoots and globally poorer current dynamics. An anti wind-up implementation, called back-calculation, proposed in [14] is applied. The references generated by the PI controllers look like (16) and (17).

$$v_{d,PI}^* = k_{p,d}((i_d^* - i_d)) + k_{i,d}((i_d^* - i_d) + \frac{1}{k_{p,d}}(v_{d,sat}^* - v_d^*))/p \tag{16}$$

$$v_{q,PI}^* = k_{p,q}((i_q^* - i_q)) + k_{i,q}((i_q^* - i_q) + \frac{1}{k_{p,q}}(v_{q,sat}^* - v_q^*))/p \tag{17}$$

The part added in the integrator only prevent the integrator output from rising when the voltage reference is saturated, but is zero otherwise and then does not affect the unsaturated behaviour.

The current controller is now fully defined. The outer torque controller that outputs the current references need to be tackled. The design presented in this paper is based on the maximum torque per ampere computation and is directly inspired by what can be found in [11], [15]. Maximum torque per ampere equation is derived by calculating the maximum torque per current magnitude:

$$\left.\frac{\partial T_{em}}{\partial i_d}\right|_{i_s=cste} = 0 \quad i_q{}^2 - i_d{}^2 - \frac{\psi}{L_d - L_q}i_d = 0 \tag{18}$$

$$i_d = \frac{\psi}{2(L_d - L_q)} - \sqrt{\left(\frac{\psi}{2(L_d - L_q)}\right)^2 + i_q{}^2} \tag{19}$$

2.2. Inverter
2.2.1. Physical model
The three phase inverter converts the continuous current voltage into an alternative current voltage that can be fed to an AC motor. Figure 2 displays the motor/inverter set up that will be modeled in this paper. The switched model takes into account the voltage harmonics i.e the motor phases are fed with a non-sinusoidal switched voltage waveform. The machine is considered balanced and Y-connected with an ungrounded neutral point. The transistors of a same leg are controlled with complementary switching signals $S_{a,b,c}$.
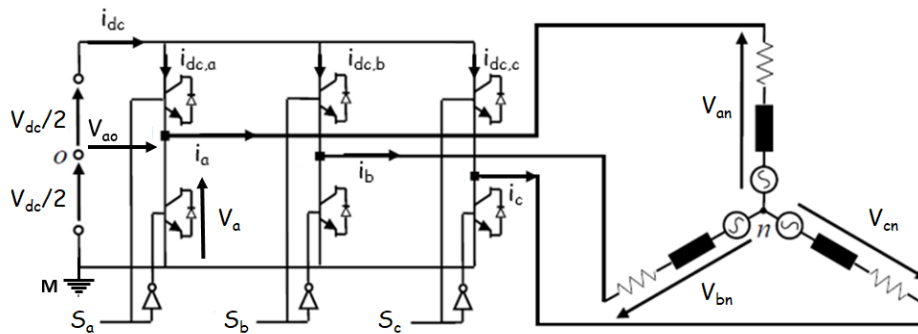
Figure 2. 3 phase AC motor with inverter

The voltages between a phase connection and the ground point M can easily be calculated. The four following equations defines the set up:

$$i_a + i_b + i_c = 0 \tag{20}$$

$$v_{an} + v_{bn} + v_{cn} = 0 \tag{21}$$

$$v_{aM,bM,cM} = S_{a,b,c} V_{dc} \tag{22}$$

$$i_{dc} = i_{dc_a} + i_{dc,b} + i_{dc,c} = S_a i_a + S_b i_b + S_c i_c \tag{23}$$

by using these equations and linear algebra one gets [16]:

$$\begin{pmatrix} v_{an} \\ v_{bn} \\ v_{cn} \end{pmatrix} = \frac{V_{dc}}{3} \begin{pmatrix} 2 & -1 & -1 \\ -1 & 2 & -1 \\ -1 & -1 & 2 \end{pmatrix} \begin{pmatrix} S_a \\ S_b \\ S_c \end{pmatrix} \tag{24}$$

this equation is true if the voltage drops across the semi-conductors are neglected, which is the case here. The matrix is of rank two, which means that there are infinite possibilities of switching patterns to obtain a given set of phase voltages. It leaves a degree of freedom which Figure 2 brings forward:

$$\begin{pmatrix} v_{a0} \\ v_{b0} \\ v_{c0} \end{pmatrix} = \begin{pmatrix} v_{an} \\ v_{bn} \\ v_{cn} \end{pmatrix} + \begin{pmatrix} v_{n0} \\ v_{n0} \\ v_{n0} \end{pmatrix} = V_{dc} \begin{pmatrix} S_a \\ S_b \\ S_c \end{pmatrix} - \frac{V_{dc}}{2} \begin{pmatrix} 1 \\ 1 \\ 1 \end{pmatrix} \tag{25}$$

V_{n0} is the voltage between the neutral point and the fictitious middle point of the continuous DC link. This is the homopolar component that appears clearly when Clarke transform [17] is applied to the phase voltages:

$$[C_{\alpha\beta0}] \begin{pmatrix} v_{an} \\ v_{bn} \\ v_{cn} \end{pmatrix} = \begin{pmatrix} v_\alpha \\ v_\beta \\ 0 \end{pmatrix} \quad ; \quad [C_{\alpha\beta0}] \begin{pmatrix} v_{a0} \\ v_{b0} \\ v_{c0} \end{pmatrix} = \begin{pmatrix} v_\alpha \\ v_\beta \\ v_{n0} \end{pmatrix} \tag{26}$$

this characteristic of the inverter is used for control purposes as explained in the control design part.

To simplify the inverter model, the switching period can be considered infinitesimal so it produces exactly the requested voltage at any time. It is exactly the same as just neglecting the voltage harmonics and considering that the motor receives only the fundamental of the switched waveform. The averaged inverter model obtained does not have any dynamics, since the inverter does not have elements that can accumulate

energy, hence no states that varies dynamically. The switching signals are reduced to their equivalent duty cycle (T_s is the controller sampling period). For a phase i:

$$d_i = \frac{1}{T_s} \int_{t_0}^{t_0+T_s} S_i dt \qquad (27)$$

finally, the equation linking the DC current with the phase currents can be rewritten for the averaged model:

$$i_{dc} = d_a i_a + d_b i_b + d_c i_c \qquad (28)$$

2.2.2. Control design

The switching signals are generated by a control scheme in order to replicate the voltage reference vdq^*_{sat} on average on a sampling period T_{sw} by switching at the right moment between two voltage reference sampling. The switching period T_{sw} can be defined as the time needed for all the transistors to do the adequate switchings and come back to their previous state. Some switching patterns called "discontinuous" allow the transistors of a leg not to switch during a period. In this paper a continuous control method is used and the transistors all switch twice in a period. A synchronous sampling is used, which means that the measured signals received by the motor current controller are sampled and transistors switching times are computed at a multiple of the switching rate. It can be at the same rate but here an asymmetrical sampling is used. It samples the incoming signals and computes the voltage references and switching times at twice the switching rate. The switching instants are not exactly symmetrical from the first half switching period to the second, hence its name. Figure 3 shows this asymmetry with the voltage reference that changes in the middle of the switching period T_{sw}. However the difference from one sample to the next is very low in practice due to a very high switching frequency compared to the motor current dynamics bandwidth.
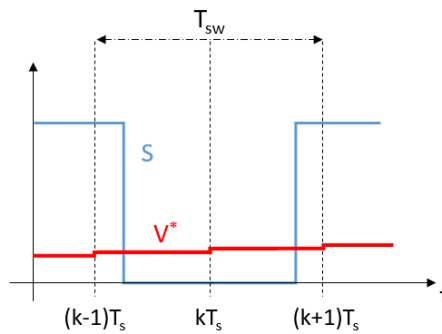

Figure 3. Switching waveform and voltage reference

3. OPEN CIRCUIT FAULTS
3.1. Faulty inverter model

A simple way to adapt the inverter model for open-circuit fault is found in [18]. The reasoning presented here is similar. In case of a fault from the transistor or its control circuit, the states of the two transistors of a leg are not correlated anymore. By building the Boolean table of a leg, one can find the way to adapt equations (22) and (23). One can refer to Figure 2 for notations. Let's note the upper and lower transistors states S_1 and S_2. The Table 1 gives the new equations true for each phase ph:

$$v_{phM} = (S_1 + \overline{S_2}(i_{ph} < 0))V_{dc} \qquad (29)$$

$$i_{dc,ph} = (S_1 + \overline{S_2}(i_{ph} < 0))i_{ph} \qquad (30)$$

Table 1. Boolean table of an inverter leg

Current	Transistors States S_1, S_2		
	S_1=0 ; S_2=1	S_1=1 ; S_2=0	S_1=0 ; S_2=0
i >0	i_{dc}=0 ; V_M=0	i_{dc}=i ; V_M=V_{DC}	i_{dc}=0 ; V_M=0
i <0	i_{dc}=0 ; V_M=0	i_{dc}=i ; V_M=V_{DC}	i_{dc}=i ; V_M=V_{DC}

3.2. FDI schemes

The FDI schemes presented here focus on OC faults detection by manipulating time signals and focusing on current monitoring. They require more lines of code in the controller and then maybe more computational power but do not need more sensors than the two current ones already available. The first technique is inspired by the work done in [19], [20]. The signals needed are the current references i_{ph}^* and the measured ones i_{ph}. Their difference e_{ph} can be averaged on an electrical period, to remove the current ripples influence, and normalized by being divided by the averaged measured current.

$$\langle i_{ph} \rangle = \frac{w_1}{2\pi} \int_{t_0}^{t_0 + \frac{w_1}{2\pi}} i_{ph} dt \tag{31}$$

$$e_{ph} = i_{ph}^* - i_{ph} \tag{32}$$

$$k_{ph} = \frac{\langle e_{ph} \rangle}{\langle |i_{ph}| \rangle} \tag{33}$$

This obtained value is then independent of the load conditions since it does not depend on the current magnitude. It equals 0 in healthy conditions because the current follows the reference. It can be compared to a fixed threshold to detect and isolate the fault. The method relies on the hypothesis that the current waveform is exactly half sinusoidal when an OC fault occurs in a leg. The value of $k_p h$ is then either 1 or -1 if the upper or lower transistor are respectively faulty [19].

The second technique relies on an observer that imitates the motor behavior by using the current state equations. It uses a constant gain which must be tuned to allow for robust detection for different operating conditions.

$$\begin{pmatrix} \frac{d\hat{i_d}}{dt} \\ \frac{d\hat{i_q}}{dt} \end{pmatrix} = \begin{bmatrix} -\frac{R_s}{L_d} & \frac{L_q}{L_d} w_r \\ -\frac{L_d}{L_q} w_r & -\frac{R_s}{L_q} \end{bmatrix} \begin{bmatrix} \hat{i_d} \\ \hat{i_q} \end{bmatrix} + \begin{bmatrix} \frac{1}{L_d} & 0 \\ 0 & \frac{1}{L_q} \end{bmatrix} \left(\begin{bmatrix} v_d \\ v_q \end{bmatrix} - \begin{bmatrix} 0 \\ \psi w_r \end{bmatrix} \right) + \begin{bmatrix} K_1 & K_3 \\ K_4 & K_2 \end{bmatrix} \left(\begin{bmatrix} \hat{i_d} \\ \hat{i_q} \end{bmatrix} - \begin{bmatrix} i_d \\ i_q \end{bmatrix} \right) \tag{34}$$

For simplicity of gain tuning, $K_1 = K_2$ and $K_3 = K_4 = 0$. Form factors are calculated for both measured and estimated currents by dividing their root mean square by their average. Both are calculated with the same equation used for previous technique and RMS is obtained just by squaring the signal before averaging. Then the difference of the form factors ff_{ph} and $\hat{ff}_{ph}$ gives residuals r_{ph} that can be compared to a threshold that must be found for robust detection purposes.

$$\langle i_{ph} \rangle_{RMS} = \sqrt{\frac{w_1}{2\pi} \int_{t_0}^{t_0 + \frac{w_1}{2\pi}} i_{ph}^2 dt} \tag{35}$$

$$ff_{ph} = \frac{\langle |i_{ph}| \rangle_{RMS}}{\langle |i_{ph}| \rangle} \tag{36}$$

$$r_{ph} = |ff_{ph} - \hat{ff}_{ph}| \tag{37}$$

In healthy conditions, the form factors both equal almost 1.11 and the residual of each phase is very close to 0. The work of [21], [22] provide active thresholds that happened to be effective in their case but ineffective in the case of the PMSM modeled in this paper, because they were always higher than the residuals even in faulty conditions, and then no fault was ever detected. Hence, they are not used in this paper. The technique proposed allows for faulty leg detection. To detect the faulty switch, one must also look at $\langle i_{ph} \rangle$ sign. If it is positive, then the faulty transistor is the lower one, and the upper one otherwise.

4.   RESULTS AND DISCUSSION

4.1.   General simulation set up

The values chosen for the stator resistance and inductance as well as the permanent magnet (PM) flux linkage are based on [14] in per unit and converted in physical values by multiplying them with the corresponding base values for three phase systems. One can verify that the physical values obtained are consistent with what is found in [13]. Besides, the switching frequency of the converters is often between 5 and 10 kHz and can

even reach 20 kHz sometimes [23]-[25]. One might notice that the switching frequency used is far above the fundamental frequency imposed by the rotor speed. By looking at the nominal values, it appears that even if the car was supposed to go at 140 km/h, twice the nominal speed, the fundamental frequency of the stator currents would be 742 Hz. The ratio between the switching frequency and the fundamental of requested currents, also called pulse number, would then be equal to 13.5 which is good enough to provide motor currents without too much harmonics. All tables used for the simulation are in shown in Tables 2-8.

Table 2. Battery and DC-link operating voltages

Parameter	Value
$V_{battery}$	400 V
$V_{DC,min}$	400 V
$V_{DC,max}$	600 V

Table 3. Base values

Base value	Formula
Z_{base}	V_n/I_n
L_{base}	$Z_{base}/w_{r,n}$
ψ_{base}	$V_n/w_{r,n}$

Table 4. Motor parameters

Parameter	Per unit	Physical value
R_s	0.02	14.7 $m\Omega$
L_d	0.6	$1.89e^{-4}$ H
L_q	1	$3.15e^{-4}$ H
ψ_m	1	99 mWb

Table 5. Converters parameters

Parameter	Value
C_{DC}	1.5 mF
L_{DC}	0.5 mH
f_{sw}	10 kHz

Table 6. Simulation parameters

Parameter	Value
Simulation time	30 s
Solver	Variable step auto (ode23t)
Throttling signal triggering	0.1 s

Table 7. Simulation parameters

Parameter	Value
Constant DC link voltage	400 V
Leg a lower transistor OC	0.2 s
Leg b upper transistor OC	0.3 s
Leg c lower transistor OC	0.4 s

Table 8. Conditions for the tests

	Initial speed = 20 km/h	Initial speed = 120 km/h
Without throttle signal transient	Test 1	Test 2
With throttle signal transient	Test 3	Test 4

4.2. Inverter with OC fault

The inverter model, with OC, and the FDI schemes to detect the defaults are presented in the mathematical model part. The Boolean used in the inverter model was first implemented in Simulink with a comparator block but it made the simulation stutter because of a very high number of comparison happening when a diode does not let the current flow. The solution found was to use an hysteresis instead to lower the number of solver calls. Then, instead of being perfectly 0, the current is flickering slightly around 0. As the simulation begins at non-zero speed, the integrators of the controllers need to catch up to reach the references and this is why the plots are all beginning at 0.1 s.

The throttle signal transient goes from 0.05 to 0.75. The parts without it simulates OC faults at low torque request, contrary to the others, which also assess the FDI schemes robustness against false alarms when confronted to fast current transients generated by the throttle signal step. Furthermore, all the tests are conducted with an external sinusoidal load of amplitude $T_n/10$, roughly equal to the load felt by the motor shaft at constant speed on a highway, and frequency $10Hz$. It is a load very unlikely to be applied to the car but it assesses the FDI schemes robustness against high transient external loads. Unless indicated, all the simulations are done with wrong parameters estimations to assess the FDI scheme robustness against parameters shifts : $R_s = 1.5\hat{R}_s$ and $L_q = 0.8\hat{L}_q$. The FDI techniques developed and implemented here are not meant to detect single leg double OC faults. A specific detection variable is used for this purpose in [19] but not here. The technique using the observer is supposed to use a specific dynamic threshold to detect and isolate a fault. However, it turns out that this threshold is always higher than the detection variable, whatever the driving conditions or the observer gain. Hence, only the detection variables are plotted. A first simulation step is conducted to verify if the transistors with anti-parallel diodes, modeled with a boolean (hysteresis in Simulink), behaves as expected. The results can be analysed afterwards.

Operating conditions of test three (Tables 2-8) are chosen to display clearly the faulty drive behaviour. Figure 4 shows that the first OC fault in the lower transistor of leg a results in a half sinusoidal current in the phase a. It is due to the lower diode that prevent negative current from flowing in the phase, as expected. The second and third OC faults impacts are difficult to analyze. The second triggers the field weakening as the controller tries to stop the current oscillations by increasing the voltage reference magnitude. These oscillations are more and more significant as the number of transistor faults increases. This creates enormous torque oscillations. It remains above 0 in average with two faults but drops when the third fault occurs.
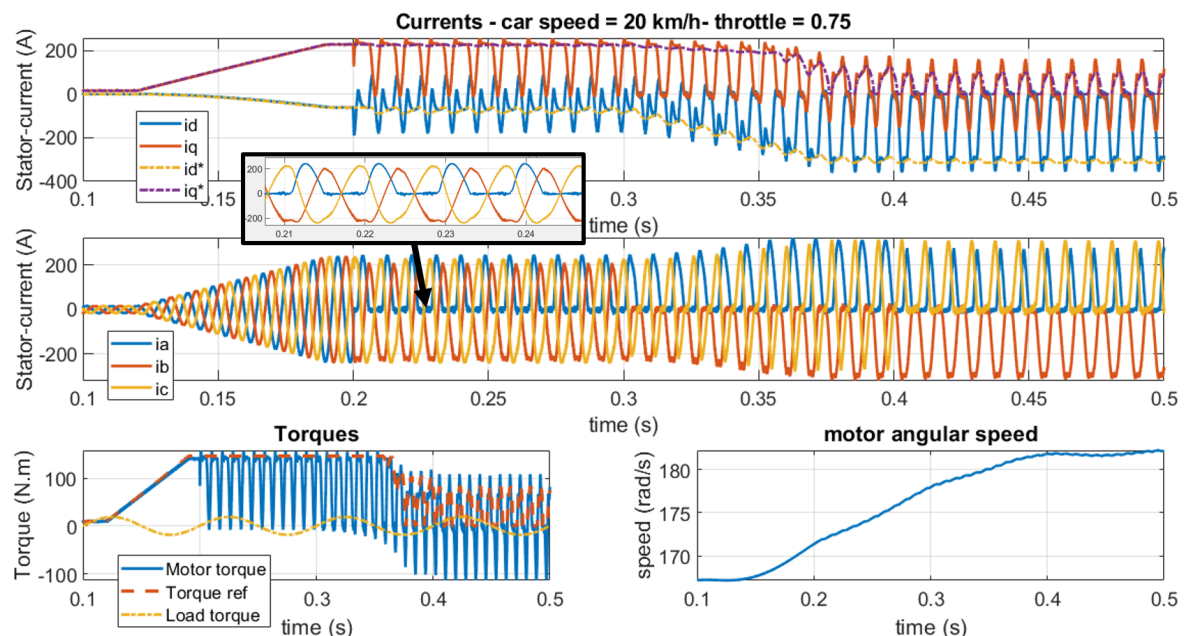

Figure 4. The First OC fault impact in the lower transistor of leg a - test 1

Figure 5 displays the plant behaviour now at high speed and low torque. Because of the high speed, the motor is already far in the field weakening region and phase currents have a high amplitude even at low torque demand. Due to the high back electromagnetic force (EMF), the phase currents are allowed to pass through the diodes that blocked them at low speed. The waveforms are then more sinusoidal. Their amplitude gets bigger and bigger as the number of fault increase, as in the previous case. However, the torque directly drops when the first fault occurs and is negative on average. In these conditions, the fault detection seems harder because of the more complex waveforms.
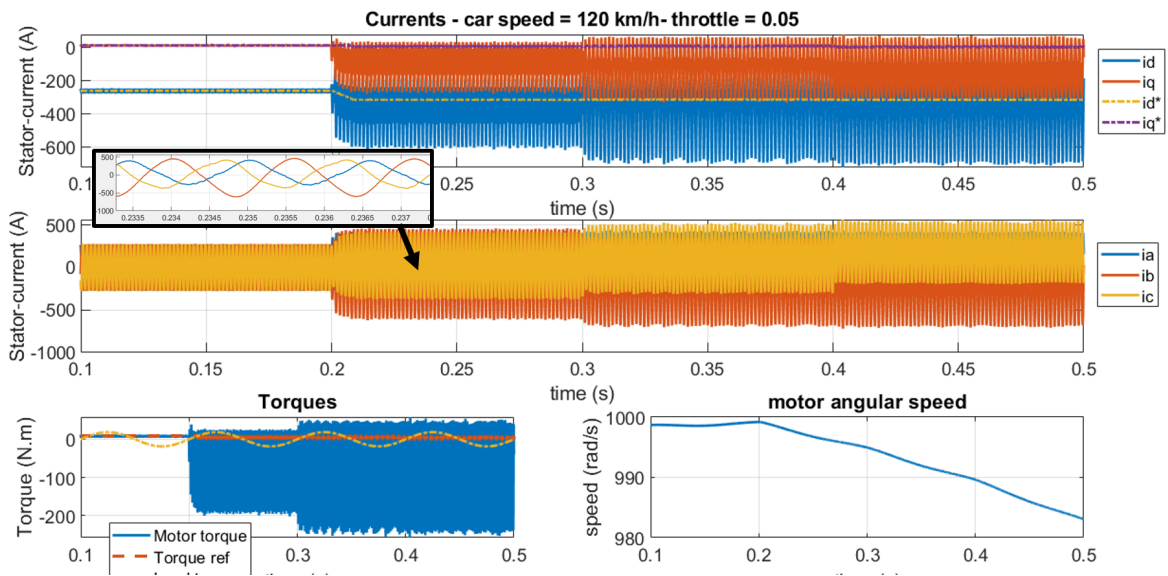
Figure 5. The second OC fault impact at high speed and low torque - test 2

The third interesting case is at low speed and low torque demand as shown in Figure 6. The amplitude of the currents is very low. In these conditions, the amplitude of phases b and c increase at each fault event whereas phase a current is almost 0 when three faults have occurred. The torque average also increases, like the amplitude of its harmonics. On the other hand, field weakening is not triggered here (one can see that the torque reference, which includes the field weakening, stays constant) because of the relatively low current spikes compared to the other scenarios. Now, the detection variables behaviour must be investigated when 1, 2, and 3 OC faults occur one by one in different legs. Three observer gain values are set for this simulation. Test 4 operating conditions are used.

Figure 7 displays the results of the observer technique when the motor parameters are well estimated and also with a higher observer gain. To have a good knowledge of the motor parameters appears to be advantageous with only one fault occurring. The healthy legs corresponding variables are very close to zero which provides a better ratio between the healthy and faulty legs variables. However, the value of the leg a variable decreases when detecting the third fault. It narrows the range of fixed thresholds that must be introduced for detection purposes.

These last test results are very close to the ones of test 2 which lead to the same analysis: The second technique manages to have the faulty leg corresponding variable clearly higher than the two others, when only one fault has occurred. But it is not the case for the first technique with d_a and d_b sharing the same absolute value when only leg a is faulty. Test 1, 2, and 3 also show that the technique with the observer is better than the other for high speed conditions. Multiple fault detection is impossible with those techniques since, when more than one fault as occurred, the variables are unpredictable and sometimes return to 0 even if their corresponding leg is faulty.
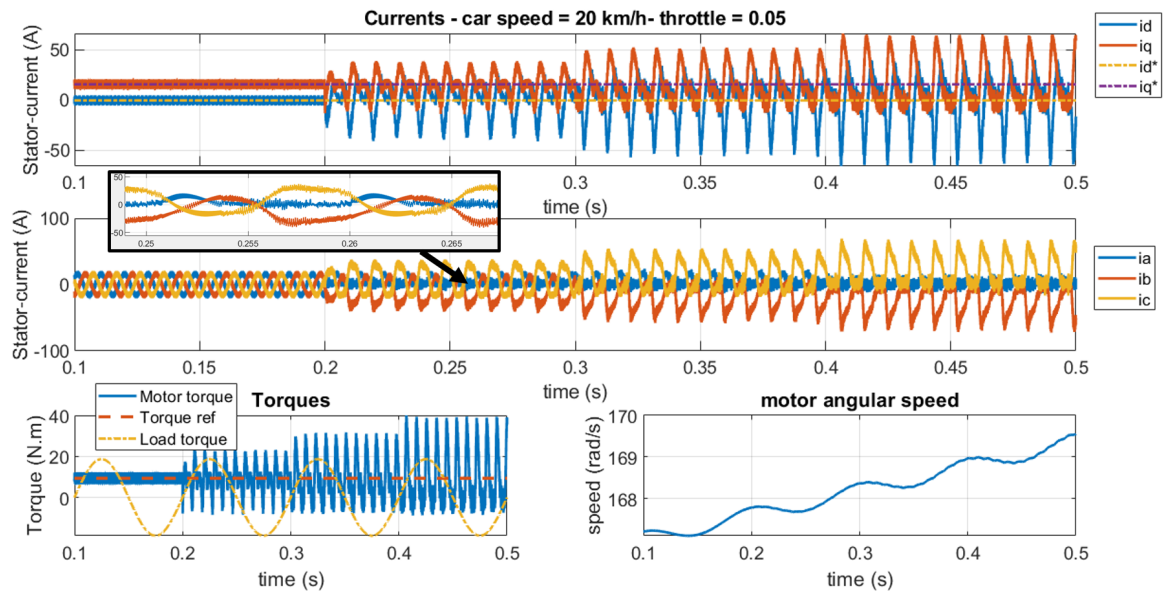
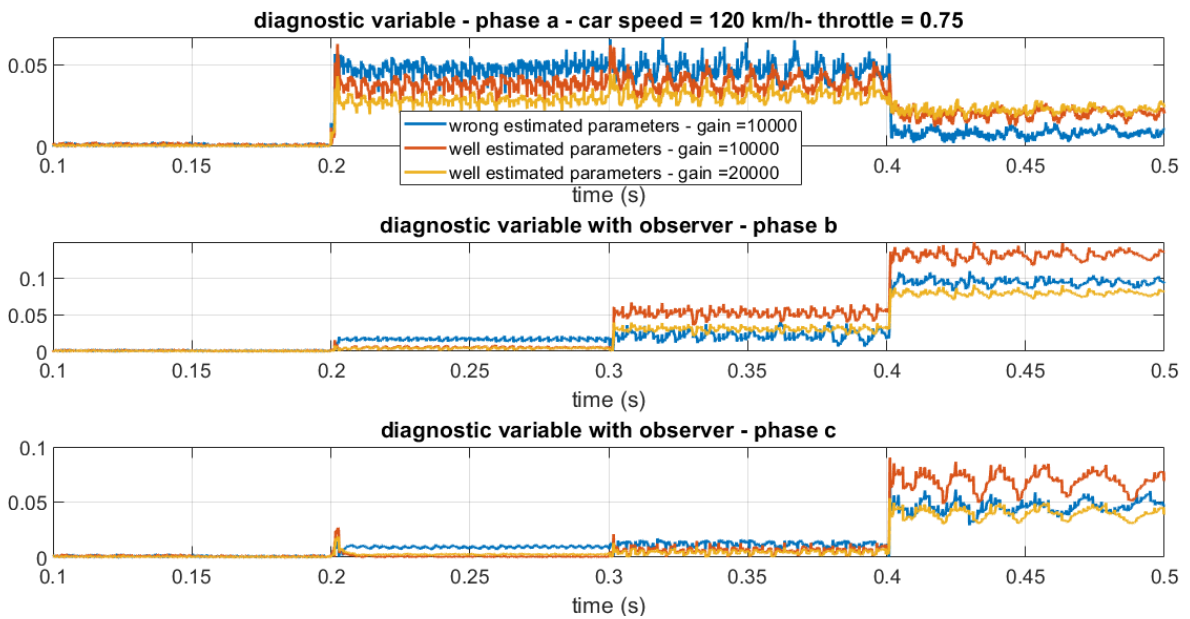Figure 6. The third OC fault impact at low speed and low torque demand - test 3

Figure 7. FDI using an observer - test 4

5.   CONCLUSION

Many faults, such as open circuits, can affect power converters and rapidly degrade the quality of the power delivered and the operation of all drive train components. During this work, new diagnostic techniques were proposed and tested to validate their efficiency. This particular techniques can detect a single leg fault within half an electrical cycle at both slow and fast speeds. This strategy requires some tuning work to find observer gains and fixed thresholds that may be overtaken by sensing variables in many driving scenarios. The electric powertrain developed here is fully defined, modeled and tested. However, there are still some issues to be resolved. For example, the model can be improved to account for non-sinusoidal flux linkages and spatial

harmonics in non-sinusoidal distributed stator windings.

AUTHOR CONTRIBUTIONS

F.H. and T.S.D contributed equally. The manuscript was written through contributions of all authors. All authors have given approval to the final version of the manuscript.

REFERENCES

[1] B. Tabbache, A. Kheloui, M. Benbouzid, A. Mamoune, and D. Diallo, "Research on fault analysis and fault-tolerant control of ev/hev powertrain," *2014 First International Conference on Green Energy ICGE 2014*, 2014, pp. 284-289, doi: 10.1109/ICGE.2014.6835436.

[2] J. Liang, K. Zhang, A. Al-Durra, S. Muyeen, and D. Zhou, "A state-of-the-art review on wind power converter fault diagnosis," *Energy Reports*, vol. 8, pp. 5341-5369, 2022, doi: 10.1016/j.egyr.2022.03.178.

[3] J. Kabziński, *Advanced control of electrical drives and power electronic converters*. Cham, Switzerland: Springer, 2016, vol. 75.

[4] Y. Xia and Y. Xu, "A transferrable data-driven method for IGBT open-circuit fault diagnosis in three-phase inverters," *IEEE Transactions on Power Electronics*, vol. 36, no. 12, pp. 13478-13488, 2021, doi: 10.1109/TPEL.2021.3088889.

[5] W. Huang, J. Du, W. Hua, W. Lu, K. Bi, Y. Zhu, and Q. Fan, "Current-based open-circuit fault diagnosis for pmsm drives with model predictive control," *IEEE Transactions on Power Electronics*, vol. 36, no. 9, pp. 10695-10704, 2021, doi: 10.1109/TPEL.2021.3061448.

[6] A. Khlaief, O. Saadaoui, M. Abassi, A. Chaari, and M. Boussak, "Open circuit fault detection and FTC for sensorless pms motor control based on the back-EMF SMO," *International Journal of Electronics*, vol. 108, no. 2, pp. 264-283, 2021, doi: 10.1080/00207217.2020.1793399.

[7] A. J. M. Cardoso, *Diagnosis and fault tolerance of electrical machines, power electronics and drives*. London, UK: The Institution of Engineering and Technology, 2018.

[8] M. Azeroual *et al.*, "Fault location and detection techniques in power distribution systems with distributed generation: Kenitra city (morocco) as a case study," *Electric Power Systems Research*, vol. 209, p. 108026, 2022, doi: 10.1016/j.epsr.2022.108026.

[9] Z. Gao, C. Cecati, and S. X. Ding, "A survey of fault diagnosis and fault-tolerant techniques—part i: fault diagnosis with model-based and signal-based approaches," *IEEE Transactions on Industrial Electronics*, vol. 62, no. 6, pp. 3757-3767, 2015, doi: 10.1109/TIE.2015.2417501.

[10] Z. Gao, C. Cecati, and S. X. Ding, "A survey of fault diagnosis and fault-tolerant techniques-part ii: fault diagnosis with knowledge-based and hybrid/active approaches," *IEEE Transactions on Industrial Electronics*, vol. 62, no. 6, pp. 3768-3774, 2015, doi: 10.1109/TIE.2015.2419013.

[11] S. Vaez-Zadeh, *Control of permanent magnet synchronous motors*. Oxford, UK: Oxford University Press, 2018.

[12] D. Campos-Delgado, D. Espinoza-Trejo, and E. Palacios, "Fault-tolerant control in variable speed drives: a survey," *IET Electric Power Applications*, vol. 2, no. 2, pp. 121-134, 2008, doi: 10.1049/iet-epa:20070203.

[13] O. Wallmark, "On control of permanent-magnet synchronous motors in hybrid-electric vehicle applications," Ph.D. dissertation, Department of Electric Power Engineering, Chalmers University of Technology, Göteborg, Sweden, 2004.

[14] L. Harnefors, M. Hinkkanen, O. Wallmark, and A. G. Yepes, "Control of voltage-source converters and variable-speed drives," *Lecture notes, Västerås, Sweden*, 2014.

[15] L. Sepulchre, M. Fadel, M. Pietrzak-David, and G. Porte, "MTPV flux-weakening strategy for PMSM high speed drive," *IEEE Transactions on Industry Applications*, vol. 54, no. 6, pp. 6081-6089, 2018, doi: 10.1109/TIA.2018.2856841.

[16] N. Patin, *Power electronics applied to industrial systems and transports, volume 2: power converters and their control*. London, UK: Elsevier, 2015.

[17] F. Giri, *AC electric motors control: advanced design techniques and applications*. Chichester, UK: John Wiley & Sons, 2013.

[18] H. Tao, T. Peng, C. Yang, Z. Chen, C. Yang, and W. Gui, "Open-circuit fault analysis and modeling for power converter based on single arm model," *Electronics*, vol. 8, no. 6, p. 633, 2019, doi: 10.3390/electronics8060633.

[19] J. O. Estima and A. J. M. Cardoso, "A new algorithm for real-time multiple open-circuit fault diagnosis in voltage-fed pwm motor drives by the reference current errors," *IEEE Transactions on Industrial Electronics*, vol. 60, no. 8, pp. 3496-3505, 2012, doi: 10.1109/TIE.2012.2188877.

[20] M. E. Elsayed, M. S. Hamad, and H. A. Ashour, "Modeling and analysis of PMSM under regenerative braking operations with fault-tolerant for EV/HEV applications," *2021 31st International Conference on Computer Theory and Applications (ICCTA)*, 2021, pp. 112-119, doi: 10.1109/ICCTA54562.2021.9916631.

[21] I. Jlassi, J. O. Estima, S. K. El Khil, N. M. Bellaaj, and A. J. M. Cardoso, "A robust observer-based method for IGBTs and current sensors fault diagnosis in voltage-source inverters of PMSM drives," *IEEE Transactions on Industry Applications*, vol. 53, no. 3, pp. 2894-2905, 2017, doi: 10.1109/TIA.2016.2616398.

[22] K. Dhibi, M. Mansouri, K. Bouzrara, H. Nounou, and M. Nounou, "Reduced neural network based ensemble approach for fault detection and diagnosis of wind energy converter systems," *Renewable Energy*, vol. 194, pp. 778-787, 2022, doi: 10.1016/j.renene.2022.05.082.

[23] T. A. Burress *et al.*, "Evaluation of the 2010 Toyota Prius hybrid synergy drive system," 2011, doi: 10.2172/1007833.
[24] O. Wallmark, *Control of permanent-magnet synchronous machines in automotive applications.* Chalmers University of Technology, 2006.
[25] P. Caillard, "Design by optimization of an electric traction chain and its control by multi-physics modeling (in French: Conception par optimisation d'une chaine de traction électrique et de son contrôle par modélisation multi-physique," M.S. thesis, Université Lille, Lille, France, 2015.

BIOGRAPHIES OF AUTHORS

Fatima Haidar holds a bachelor's degree, a Master's degree, and a Ph.D. degree in Physical Chemistry of Materials from Montpellier University in France since 2018. She was a Postdoctoral Researcher and an invited lecturer in several French institutes in the field of chemistry, fuel cells and motors. She is currently a Work Package Leader on Fuel Cells and Motors in the Research and Innovative department, at Capgemini Engineering. Her research interests include powertrains, physical chemistry of materials, conversion/storage devices, simulation, data-driven modeling, fault diagnosis, fault-tolerant control, renewable energy systems, power electronics, hybrid and electrical vehicles. She can be contacted at email: Fatima.haidar@capgemini.com.

Takwa Sallemi Douiri holds a bachelor's degree and Master's degree, and Ph.D in Electrical Engineering specialized in fault diagnosis of electrical motors and wind turbines from Cergy-Pontoise University in France and the International Engineering School of Monastir in Tunisia, since 2017, besides several certifications and skills. She taught many engineering courses and has many published papers in different Journals. She has joined Capgemini Engineering, as a consulting engineer three years ago. Her research fields include fault detection and compensation in fault diagnosis, power converters and motors. She can be contacted at email: sellami.takwa8@gmail.com.

Thomas Bartoli holds a Ph.D. degree in Materials Science and Engineering from Paris-Est University in France since 2019. He has joined Capgemini Engineering, as a consulting engineer three years ago. He is currently an expert in the simulation of Batteries, power converters and Motors in the Research and Innovative department, at Capgemini Engineering. His research interests include powertrains, physical properties of materials, storage devices, simulation, renewable energy systems, power electronics, hybrid, and electrical vehicles. He can be contacted by email at thomas.bartoli@capgemini.com